Nonlocal hydrodynamic model for gravity-driven transport in nanochannels

Arghyadeep Paul[1*] and N. R. Aluru[2]

[1]*Department of Mechanical Science and Engineering, Beckman Institute for Advanced Science and Technology, University of Illinois at Urbana−Champaign, Urbana, Illinois 61801, United States*

[2]*Walker Department of Mechanical Engineering, Oden Institute for Computational Engineering and Sciences, The University of Texas at Austin, Austin, Texas 78712*

ABSTRACT

It has been established that Newton's law of viscosity fails for fluids under strong confinement as the strain-rate varies significantly over molecular length-scales. We thereby investigate if a nonlocal shear stress accounting for the strain-rate of an adjoining region by a convolution relation with a nonlocal viscosity kernel can be employed to predict the gravity-driven isothermal flow of a Weeks-Chandler-Andersen (WCA) fluid in a nanochannel. We estimate, using the local average density model (LADM), the fluid's viscosity kernel from isotropic bulk systems of corresponding state points by the Sinusoidal Transverse Force (STF) method. A continuum model is proposed to solve the nonlocal hydrodynamics, whose solutions capture the key features and agree qualitatively with the results of non-equilibrium molecular dynamics (NEMD) simulations, with deviations observed mostly near the fluid-channel interface.

I. INTRODUCTION

Sufficiently large strain-rate variations over length-scales of the order of molecular dimensions in nanochannel flows makes the use of local Newtonian shear stress relation questionable.[1-7] Due to high density gradients, such fluids experience large viscosity variations. Here, using the Newtonian relation with a local position-dependent viscosity poses difficulties due to the presence of singularities[2,3] where the strain-rate is zero, but the shear stress is not. Evans and Morriss[1] introduced the nonlocal shear stress as a convolution function of strain-rates over the fluid region with a generalized nonlocal viscosity kernel accounting for both spatial and temporal nonlocality,

$$\tau\left(r,t\right)=\int_{0}^{t}\int_{-\infty}^{\infty}\mu\left(r-r',t-t'\right)\dot{\varepsilon}\left(r',t'\right)dr'dt' \tag{1}$$

***Corresponding Author**: Arghyadeep Paul, E-mail: paul26@illinois.edu

where $\tau(r,t)$ and $\dot{\varepsilon}(r,t)$ are the stress and strain-rate at position r and time t and μ is the nonlocal viscosity kernel. Interestingly, eq. (1) can mathematically explain the aforementioned singularities. Assuming a steady-state, eq. (1) reduces to:

$$\tau(r) = \int_{-\infty}^{\infty} \mu(r-r')\dot{\varepsilon}(r')dr', \tag{2}$$

where the strain-rate at a point r' affects the shear stress at another point $r \neq r'$, due to interparticle correlations. However, eq. (2) is valid only for homogeneous fluids with a uniform density and must be modified (see Sec. II) to model the flow of inhomogeneous dense fluids in nanochannels. Previous studies[8-11] have explored the effects of density variations due to external forces modulated sinusoidally in both the transverse and longitudinal directions (STF-SLF methods) on unconfined fluid-flow. But such artificially induced inhomogeneities differ from those generated by fluid-wall interactions in nanochannels, where further analysis of the microscopic hydrodynamics equations and boundary conditions at the interface is needed.[12-14] We, however, aim for simpler techniques to estimate the nanochannel flow solving eq. (2), which for an inhomogeneous fluid requires the viscosity kernel ~~of the fluid~~ to be position dependent. Past attempts to extract such a kernel of bounded systems have been inaccurate due to abundant challenges,[3,~~8,9~~15,16] while deriving the nonlocal viscosity kernel of homogeneous fluids, via the STF method[17-20] or Green-Kubo Formula,[21] has been demonstrated to great effects.[~~10-12~~] Applying LADM,[22-24] a set of such isotropic kernels over a range of thermodynamic variables can be used as an approximate substitute to the viscosity kernel of an inhomogeneous system of the fluid displaying the same range of local thermodynamic variables in space. Using such parametrized inputs to solve nonlocal viscous hydrodynamics in a continuum model has remained unexplored for non-homogeneous systems at nanoscale.

Our objective in this study is to investigate whether the nonlocal constitutive shear stress relation can predict the nanochannel flow of a simple fluid whose particles interact by the Weeks-Chandler-Andersen (WCA) potential[~~13~~25] and its nonlocal viscosity kernel is derived using the STF procedure.[~~14~~20] A model of nonlocal transport equations is set up to describe the gravity-driven flow in a nanochannel with a width of the order of intermolecular correlations. With this transport model, we develop a simple method in the continuum regime that can predict fluid-flows in the nanoscale domain. The rest of the article is organized as follows: In Sec. II, we elaborate the

equations of nonlocal hydrodynamics for the fluid-nanochannel system under study. In Sec. III, we present a continuum model and discuss the parametrized inputs for it. In Sec. IV, we present the results and discuss them in detail. Sec. V presents concluding remarks.

II. PROBLEM FORMULATION

The nonlocal constitutive relation in eq. (2) is defined for homogeneous fluids, where the viscosity kernel is an even function of the distance ($r - r'$) between the point where the shear stress is measured and the point whose strain-rate is considered. Such kernels~~, separated into the local viscosity μ_o and a nonlocal weight function f,~~ were parametrically derived ~~and constructed~~ by Travis et al.,~~[10]~~[17] ~~and~~ Hansen et al.~~[11]~~[18] and Todd et al.[26], and written as a product of local viscosity μ_o and a nonlocal weight function f for mathematical convenience, such that

$$\int_{-\infty}^{\infty} \mu(r-r')\,dr' = \int_{-\infty}^{\infty} \{\mu_o(r) f(r-r')\}\,dr' = \mu_o(r)~~,~~, \tag{3}$$

and the integration of f across space results in 1. If the kernel is a Dirac-delta function about r, the nonlocal relation becomes the local Newtonian relation. This approximation is good, for example, in macroscopic bulk flows where the strain-rate remains constant across the kernel width. The nonlocal constitutive shear stress relation can hence be interpreted as a general theory.

In this study, we consider a nanochannel with walls in the xy-plane separated by a width of L in the z-direction, taking the mid-plane between them as $z = 0$. The non-homogeneous WCA fluid is subjected to a uniform gravity g_o in the x-direction at temperature $T = 107.52$ K. Since the fluid in the nanochannel is inhomogeneous, the nonlocal viscosity kernel cannot be treated as an isotropic or homogeneous entity and must vary with position, modifying eq. (2) to

$$\tau(r) = \int_{-\infty}^{\infty} \mu(r, r-r')\,\dot{\varepsilon}(r')\,dr'. \tag{4}$$

For the nanochannel system considered here, eq. (4) can be simplified to

$$\tau(z) = \int_{-\infty}^{\infty} \mu(z, z-z')\,\dot{\varepsilon}(z')\,dz', \tag{5}$$

where $\mu(z, z-z')$ further separates into a local and a nonlocal part (similar to eq. (3)) as

$$\mu(z, z-z') = \mu_o(z) f(z, z-z'), \tag{6}$$

~~As per eq. (3), integrating the nonlocal weight function *f* in space must result in unity.~~ The shear stress in the nanochannel is derived by integrating the momentum conservation equation under a steady-state condition in eq. (7), where m is the mass of the fluid particles and $\rho(z)$ is the local density profile obtained from the non-equilibrium molecular dynamics (NEMD) simulation of the nanochannel flow (described in Sec. III.B).

$$\tau(z) = -mg_o \int_0^z \rho(z')\,dz'. \tag{7}$$

Due to symmetry, the shear stress at the channel centreline $z = 0$ is taken to be zero. Eqs. (5), (6) and (7) are used in Sec. III.D to build the continuum model. Several such quasi-continuum models have been reported in the literature previously,[~~15-19~~27-31] albeit not with nonlocal transport equations.

III. METHODS

A. Extraction of the Nonlocal Viscosity Kernel:

Calculating the viscosity kernel of a bounded inhomogeneous fluid can be rife with inaccuracies. As an alternative, we obtain the nonlocal viscosity kernel of unconfined homogeneous fluids with densities taken from the local average density (LAD) profile of the WCA fluid in the nanochannel, obtained by the NEMD simulations in Sec. III.B. Such a kernel, derived at a specific density, is then used as a substitute for the viscosity kernel at a position in the channel having an equal LAD. This is the LAD model (LADM) where the transport coefficients in a non-homogeneous fluid at a position are shown to be those of a homogeneous fluid with a density equal to the average of the local density around that position in the inhomogeneous fluid over a molecular volume.[~~20-22~~22-24]

The STF procedure is used to obtain the isotropic viscosity kernels, where wavenumber dependent viscosities are computed in the Fourier (k) space for homogeneous fluids subjected to sinusoidal gravity-fields of varying amplitudes and wavelength. For each wavelength, the k-space viscosities are extrapolated to a zero strain-rate (or gravity) limit,[~~10,11~~17,18] which are plotted against wavenumber, fit to a curve, and inverted to real-space to get the kernels. As mentioned earlier, this is done for various densities. Here, we subject a bulk homogeneous fluid of density ρ_o to a gravity g_x in the streamwise direction, x, that is sinusoidally modulated in a direction transverse to the flow, z.

$$g_x(z) = g_o \sin(k_n z) \tag{8}$$

The wavenumber k_n can be written as ($2\pi n/L_o$) where L_o is the length of the fluid domain in z direction and n = 1, 2, 3, …. depicting the different wavelengths (L_o/n). A fundamental way to obtain the nonlocal viscosity kernel is to apply the Convolution theorem to eq. (2), which gives

$$\bar{\tau}(k_n) = \bar{\mu}(k_n)\bar{\dot{\varepsilon}}(k_n), \tag{9}$$

where the Fourier transform of shear stress is simply a product of those of the nonlocal viscosity kernel and strain-rate. Taking Fourier transforms of the steady-state momentum conservation equation for a homogeneous fluid and of the strain-rate definition yields

$$\bar{\tau}(k_n) = -im\rho_o \bar{g}(k_n)/k_n\,, \tag{10}$$

$$\bar{\dot{\varepsilon}}(k_n) = -ik_n \bar{u}(k_n). \tag{11}$$

As a result, the wave-vector dependent viscosity in the Fourier-space is

$$\bar{\mu}(k_n) = \frac{\bar{\tau}(k_n)}{\bar{\dot{\varepsilon}}(k_n)} = \frac{m\rho_o \bar{g}(k_n)}{k_n^2\{\bar{u}(k_n)\}}. \tag{12}$$

Here, the Fourier coefficient of the gravity-field (at wavenumber k_n) is g_o by definition and the Fourier-coefficient of the velocity field at k_n is obtained by the discrete Fourier Sine transform of the velocity profile obtained by NEMD simulation of an unconfined homogeneous fluid of density ρ_o (described in Sec. III.C) with N particles in the simulation box

$$\bar{u}(k_n) = [2/N]\sum_{i=1}^{N} \sin(k_n z_i) v_{x,i}\,, \tag{13}$$

where z is the particle position, v_x is the streamwise velocity and i is the particle index. It must be noted that eq. (12) is valid only in the limit of zero strain-rate, as the Fourier transforms of shear stress and strain-rate contain terms with higher harmonics at large gravity-field amplitudes g_o[10,11,17,18]. Therefore, the k-space viscosities are extrapolated to the zero strain-rate limit for each wavenumber by fitting them into the Quentrec local order theory[10,17]

$$\bar{\mu}(k_n, \bar{\dot{\varepsilon}}) = \bar{\mu}(k_n, 0) + \left[a\bar{\dot{\varepsilon}}^2 \Big/ \left(\bar{\dot{\varepsilon}}^2 + b\right)\right]. \tag{14}$$

Once the zero strain-rate limiting values are computed, their dependence on the wavenumber k_n is plotted (see Fig. 1(a)) and fit using either a Gaussian curve[18] with the parameters σ_1 and σ_2,

$$\bar{\mu}(k_n) = \frac{\mu_o}{2}\left[\exp\left(\frac{-k_n^2}{2\sigma_1^2}\right) + \exp\left(\frac{-k_n^2}{2\sigma_1^2}\right)\right] \tag{15}$$

or a Lorentzian curve[18] with the parameters α and β,

$$\bar{\mu}(k_n) = \mu_o \Big/ \left(1 + \alpha |k_n|^{\beta}\right). \tag{16}$$

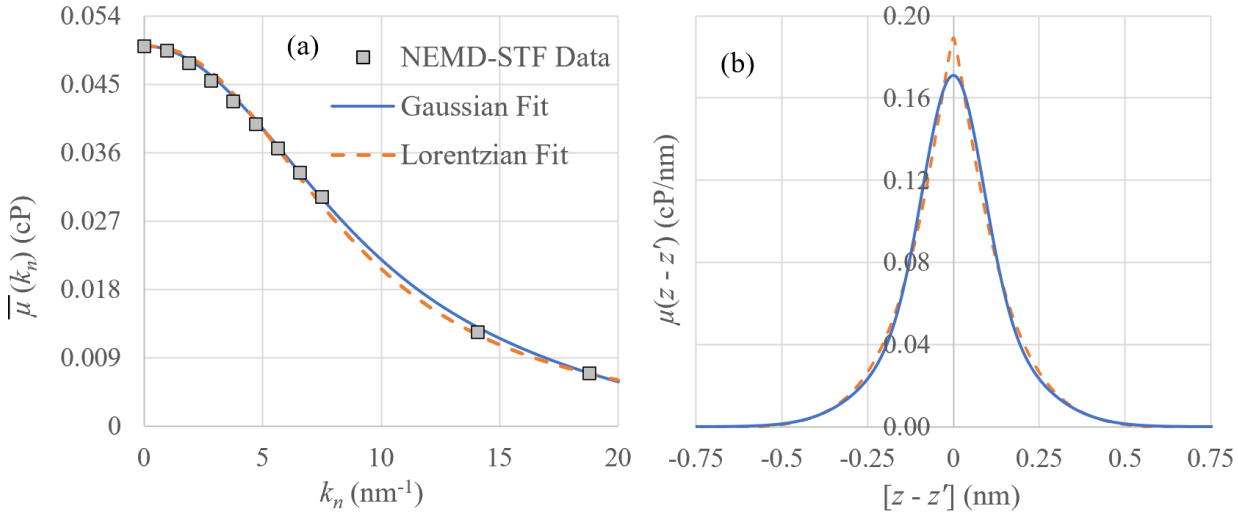

Figure 1: (a) Wavevector dependence of the zero-field k-space viscosity of the unconfined homogeneous WCA fluid at ρ_o = 12.62 particles/nm^3 and T = 107.52 K. The squares represent NEMD-STF data, the blue (solid) line is the Gaussian curve fit using eq. (15), where σ_1 = 5.42396 nm^{-1} and σ_2 = 11.7046 nm^{-1}, and the orange (dashed) line is the Lorentzian curve fit using eq. (16), where α = 0.0063863 and β = 2.3436955. (b) The isotropic nonlocal viscosity kernel resulting from the inverse Fourier transform of the Gaussian and Lorentzian fitting curves in (a) are shown by the blue (solid) and the orange (dashed) line respectively.

These expressions fit the NEMD data well and when separated into μ_o and f (as mentioned in Sec. II), the integration of f over space yields one with negligible errors for both the fits. Meanwhile the local viscosity μ_o at density ρ_o is calculated by applying Green-Kubo relations to the stress tensor data of equilibrium molecular dynamics (EMD) simulations of unconfined homogeneous systems (see Sec. III.C). The parameters μ_o, σ_1, σ_2, α and β are all functions of ρ_o. The real-space nonlocal viscosity kernels are then extracted in Fig. 1(b) by an inverse Fourier transform of eqs. (15) and (16). For the Gaussian fit, this can be done analytically and results in

$$\mu(\rho_o, z-z') = \frac{\mu_o(\rho_o)}{2\sqrt{2\pi}}\left[\sigma_1(\rho_o)\exp\left(\frac{-\left(\sigma_1(\rho_o)\{z-z'\}\right)^2}{2}\right) + \sigma_2(\rho_o)\exp\left(\frac{-\left(\sigma_2(\rho_o)\{z-z'\}\right)^2}{2}\right)\right] \quad (17)$$

When using eq. (17) for confined fluids, ρ_o is replaced by LAD at the shear stress evaluation point z, based on LADM,[22-24] explaining the added dependence of μ on z in eqs. (5) and (6). The non-analytical inverse Fourier transform of the Lorentzian fit, however, is computed by Simpson's rule ~~and shows a greater nonlocality of the viscosity kernel compared to eq. (17)~~.

B. Non-equilibrium Molecular Dynamics (NEMD) Simulations of the Confined System:

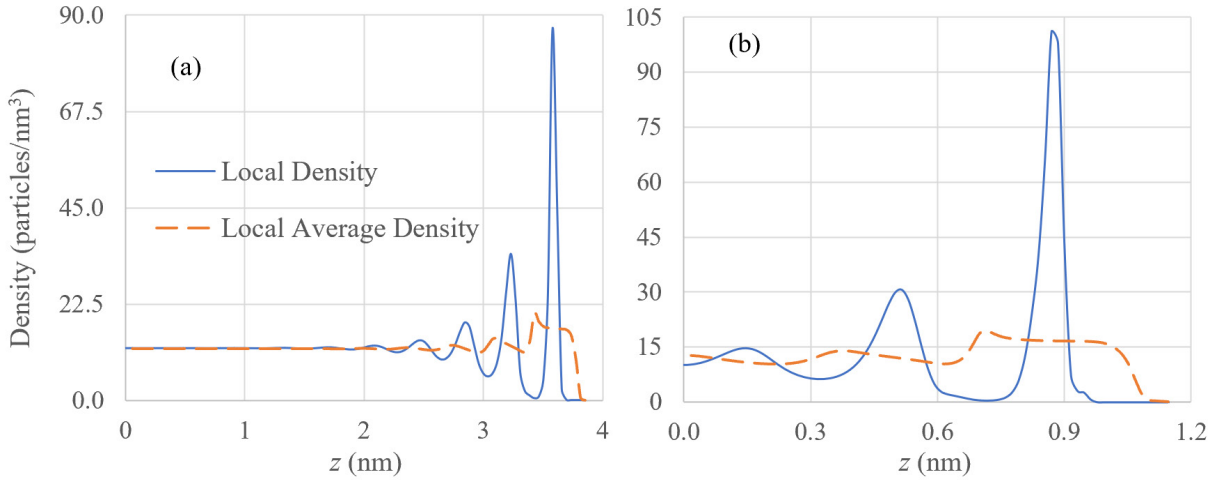

Figure 2: The fluid density profiles across half-sections of (a) the wide and (b) the narrow nanochannel. The blue (solid) and the orange (dashed) lines depict the local density and the LAD respectively.

To test the proposed continuum model, we obtain the velocity profile in the nanochannel using NEMD simulations on a system of fluid particles interacting via the short-range repulsive WCA potential[~~13~~25] between diamond latticed walls with 5 layers of Si atoms (lattice constant of 0.543 nm), having a lateral length of 4.43 nm each in the x and y directions. Two nanochannel widths (along z) were chosen: L = 7.739 nm and 2.3081 nm. An overall density of 12.62 particles per nm^3 dictated the number of fluid particles in the system. A Nose-Hoover thermostat[~~23~~32] was used to maintain the fluid at 107.52 K. The simulation b[ ]as periodic only in the x and y directions. The fluid-fluid WCA interaction corresponded to the Lennard-Jones (LJ) parameters of methane[~~15~~27] ϵ

= 1.2314 kJ/mol and σ = 0.381 nm. The fluid-wall interaction was modelled by the methane-silicon LJ potential,[15][27] ϵ = 1.7377 kJ/mol and σ = 0.3597 nm. Uniform gravities g_o = 0.0005 nm/ps^2 and 0.04 nm/ps^2 were applied on the fluid for the wide and narrow channel, respectively, while the wall atoms were fixed. Bernardi et al.[33] note that thermostatting the fluid (with fixed wall atoms) can cause velocity fluctuations at the fluid-wall interface, compared to when only the wall atoms are thermostatted. However, we do not find such effects in our NEMD velocity profiles (shown in Fig 6) where the velocity varies smoothly at the interface. Initially, the simulation was run for 4 ns to develop a steady-state fluid-flow. Then, we recorded the fluid particles' coordinates and velocities for 50 ns at a frequency of 100 fs, with a time-step of 1 fs. For accuracy, the simulations were run for 5 different initial-state ensembles. These simulations also generate the fluid density profiles in the nanochannels, needed for eq. (7) and (21), shown in Fig. 2.

C. Molecular Dynamics simulations of unconfined bulk fluids:

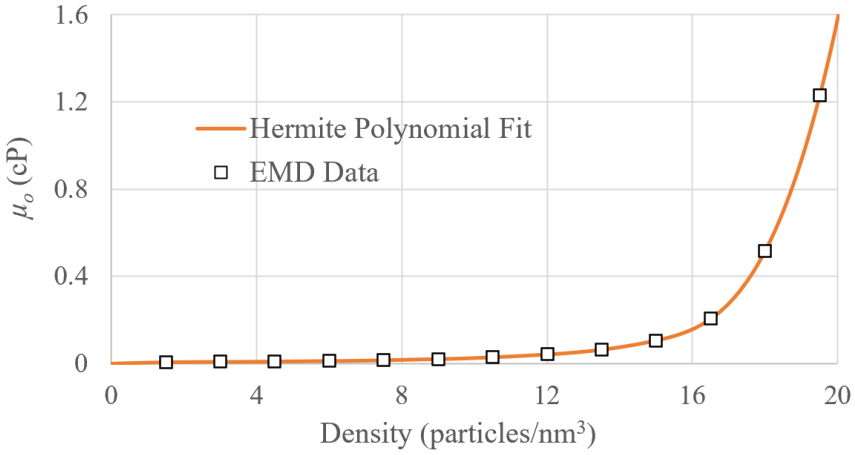

Figure 3: Density dependence of the local viscosity of the homogeneous WCA fluid at T = 107.52 K. The squares represent EMD data, while the orange (solid) line is the Hermite Polynomial fitting curve.

We consider homogeneous systems of the same fluid particles in a simulation box of length L_o = 6.7 nm with periodic boundary conditions in each direction. Different densities across the density range in the LAD profile of the nanochannel fluid (as obtained in Fig. 2) were selected, based on which the number of fluid particles varied in the simulation box. The temperature was set at 107.52 K by a Nosè-Hoover thermostat.[23][32] We performed EMD simulations to equilibrate these systems for 5 ns and collect the stress tensors for 100 ns at every time-step. Their autocorrelation functions, computed in blocks of 5 ps, were averaged around a million times to find the viscosity using the Green-Kubo relation. Then, NEMD simulations were executed on the same systems with a gravity

applied in the x-direction that is modulated sinusoidally in the z-direction with wavelengths of L_o/n (n = 1, 2, 3 … 15) to find the k-space viscosities and execute the STF analysis described in Sec. III.A. The systems developed a steady state in 4 ns, following which the coordinates and velocities of the particles were recorded for 50 ns at a frequency of 100 fs to be used in eq. (13). For accuracy, both the EMD and NEMD simulations were carried out for 5 initial-state ensembles with a time-step of 1 fs and their post-processed results are shown in Figs. 3, 4 and 5.

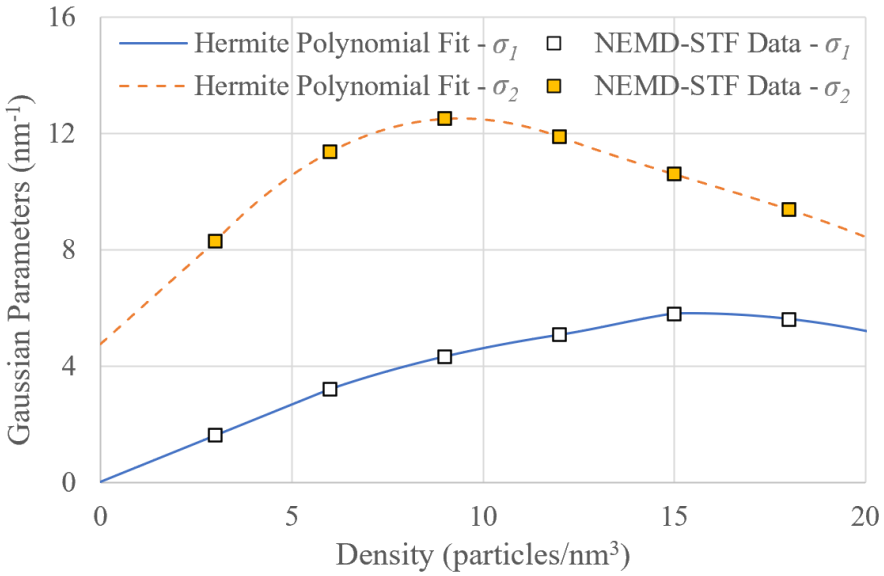

Figure 4: Density dependence of the parameters σ_1 and σ_2 in the Gaussian fitting curve, eq. (15), for the homogeneous WCA fluid at T = 107.52 K. The squares represent NEMD-STF data. The blue (solid) and the orange (dashed) lines are the Hermite Polynomial fitting curves for σ_1 and σ_2 respectively.

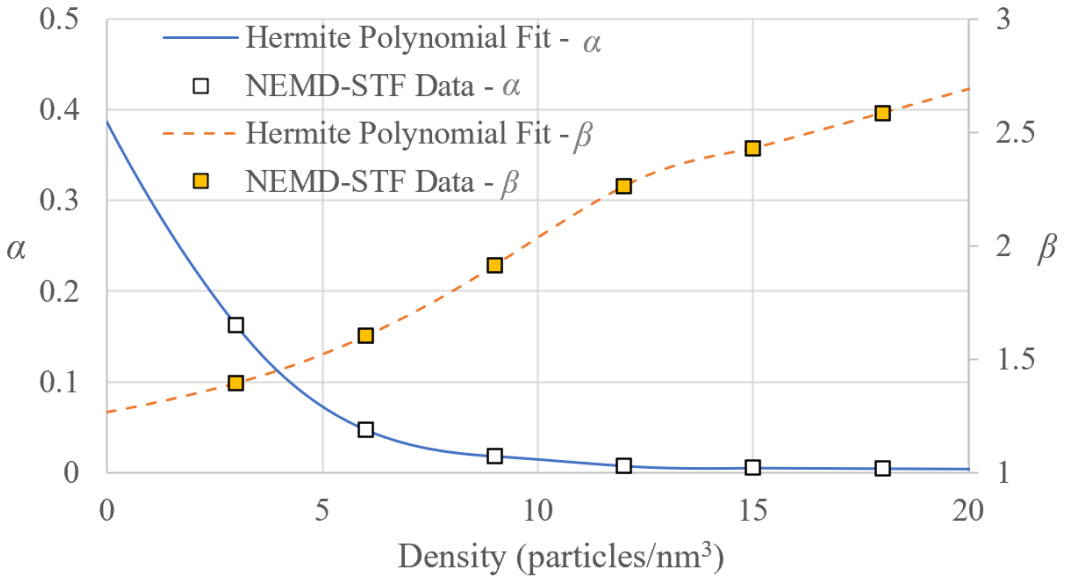

Figure 5: Density dependence of the parameters α and β in the Lorentzian fitting curve, eq. (16), for the homogeneous WCA fluid at $T = 107.52$ K. The squares represent NEMD-STF data. The blue (solid) and the orange (dashed) lines are the Hermite Polynomial fitting curves for α and β respectively.

D. Continuum Transport Model:

Here, we formulate an iterative algorithm to predict the velocity profile in the nanochannel using the nonlocal relation of shear stress τ. If τ is fragmented into a local Newtonian element

$$\tau_L(z) = \mu_o(z)\left.\frac{\partial u(z')}{\partial z'}\right|_z, \tag{18}$$

and a deviatoric element τ_D, the later can be quantified through eq. (7) and (18) as

$$\tau_D(z) = \left[-m\int_0^z g_o\rho(z')dz'\right] - \mu_o(z)\left.\frac{\partial u(z')}{\partial z'}\right|_z. \tag{19}$$

and also, by applying eq. (5), (6) and (18), we have

$$\tau_D(z) = \mu_o(z)\left[\left\{\int_{-\infty}^{\infty} f(z, z-z')\left.\frac{\partial u(z')}{\partial z'}\right|_z dz'\right\} - \left.\frac{\partial u(z')}{\partial z'}\right|_z\right]. \tag{20}$$

The two above forms of τ_D are used to build the iterative scheme presented below.

Algorithm:

(1) Inputs: The fluid density profile $\rho(z)$ in the nanochannel, the variation of the nonlocal viscous kernel parameters μ_o, σ_1, σ_2, α and β with density and relaxation factor α_r.

(2) The LAD profile $\rho_{AVE}(z)$ in the nanochannel is obtained by averaging the density across the length of a molecular diameter or the fluid-fluid WCA parameter σ, shown in Fig. 2.

$$\rho_{AVE}(z) = \frac{1}{\sigma}\left[\int_{z-(\sigma/2)}^{z+(\sigma/2)} \rho(z')\,dz'\right] \tag{21}$$

(3) Calculate the shear stress profile using eq. (7), to avoid doing so in every iteration.

(4) Set the initial guess value of the velocity profile $u(z)$: We substitute the shear stress profile (from step (3)) into the local stress relation of eq. (18) to obtain the initial guess value $u^{(0)}(z)$. To do so, we also use the boundary condition:

$$u\left(\pm\frac{L}{2}\mp\delta\right) = u_{slip}\,. \tag{22}$$

The slip velocity u_{slip} and δ are obtained by the NEMD simulations in Sec. III.B.

(5) Set the no. of iterations completed to $k = 0$ and a tolerance $\Delta \approx 10^{-3}$.

(6) Iteration begins: Do ….

i. Calculate $[\tau_D(z)]^{(k)}$ using $u^{(k)}(z)$ in eq. (20).

ii. Calculate $u^{(k+1)}(z)$ using eq. (19) by applying $[\tau_D(z)]^{(k)}$ (from step (6.i)), the shear stress profile (from step (3)) and the boundary conditions given in eq. (22).

In steps (6.i) and (6.ii), the local viscosity μ_o, viscous parameters of f, i.e. either σ_1 and σ_2 if using the Gaussian fit, or α and β if using the Lorentzian fit, at a position z in the channel are functions of $\rho_{AVE}(z)$, i.e., the LAD at z, based on the relations shown in Figs. 3, 4 and 5.

iii. Calculate the Residual $R = \frac{1}{N}\sqrt{\sum_{i=1}^{N}\left(\frac{u^{(k+1)}(z_i) - u^{(k)}(z_i)}{u^{(k)}(z_i)}\right)^2}$.

iv. Relaxation step: $u^{(k+1)} = u^{(k)} + \alpha_r[u^{(k+1)} - u^{(k)}]$. We take the value of $\alpha_r \approx 0.5$.

v. $k = k + 1$.

…… while $R > \Delta$.

IV. RESULTS AND DISCUSSIONS

We now examine the performance of our nonlocal transport model and the nonlocal viscosity kernel approximated using LADM. We investigate two different channels for the gravity-driven

flow, one wide enough to impede the development of local extrema in the velocity profile and the other narrow enough to ensure their presence.

Fig. 6(a) demonstrates that the velocity profiles predicted by both the nonlocal and local (Newtonian) theory agree well with the NEMD velocity profile for the wide channel, which does not contain any singular point or local extrema apart from the mid-channel peak. For the narrow channel, however, the local model fails altogether. Not only is it unable to capture the local extrema in the velocity profile near the interface, but it also fails to replicate the NEMD velocities and their gradients near the central part of the channel, as shown in Figs. 6(b) and 7(b). The nonlocal framework is able to mimic the local extrema near the interface of the narrow channel and agrees overall with the velocity profile obtained by the NEMD simulations to a much better extent than the local theory as seen in Fig. 7(a), with notable exceptions only in the relatively small shaded regions. It further captures the gradients of the NEMD velocity profile in the central channel region besides replicating the sign reversals in the interfacial strain-rates, as seen in Fig. 7(b), both of which the local model cannot. Moreover, the nonlocal viscosity kernels formulated using both the Gaussian and Lorentzian expressions are observed to work equally well. As a result, our nonlocal continuum transport model is able to capture most of the characteristics of the gravity-driven flow in nanochannels.

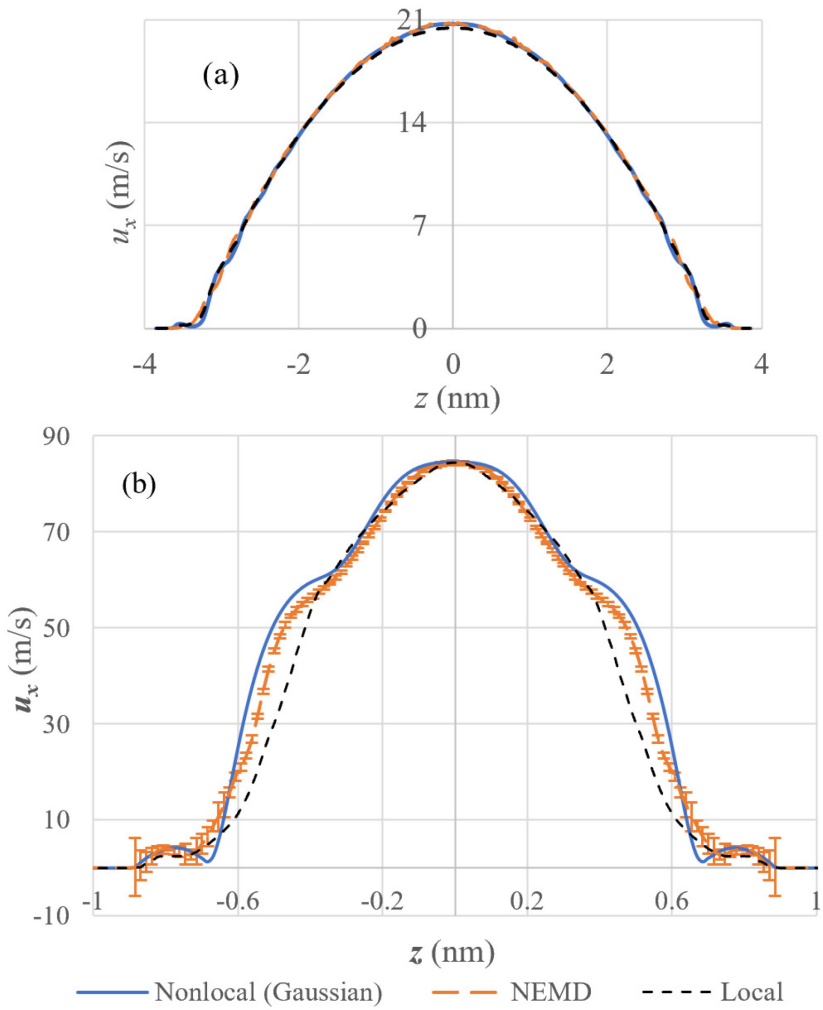

Figure 6: The velocity profiles computed by the nonlocal transport model in (a) the wide and (b) the narrow channel, are compared against those obtained by the NEMD simulations and the local theory. The blue (solid), orange (dashed) and ~~grey~~black (smaller dashed) lines are the nonlocal, reference NEMD and local velocity profiles respectively. ~~Their strain-rates profiles are shown in Fig. 7.~~

However, we still observe quantitative deviations near the interface between the nonlocal model and the NEMD velocity profile in the smaller channel. This can be attributed to a wide array of reasons. Firstly, when using the nonlocal constitutive relation at the vicinity of the interface, strain-rates on one side of the kernel width are absent, which induces errors in computing the shear stress. Secondly, the nonlocal viscosity kernel of the inhomogeneous fluid was estimated by LADM, and isotropic kernels were employed instead. In addition, these kernels were represented in Fourier space with analytical expressions as an assumption. ~~This~~ All these would lead to inaccuracies. Inhomogeneities are brought about by high gradients in density near the interface and as a result, maximum deviations between the results of the nonlocal model and NEMD

simulations are seen in that region implying that LADM fails the most near the interface. Furthermore, although the nonlocal viscosity kernels were extracted in the zero strain-rate or gravity-field limit, they were later used in our transport model under finite to large magnitudes of gravity. Consideration of these factors can improve the continuum transport framework discussed in this paper.

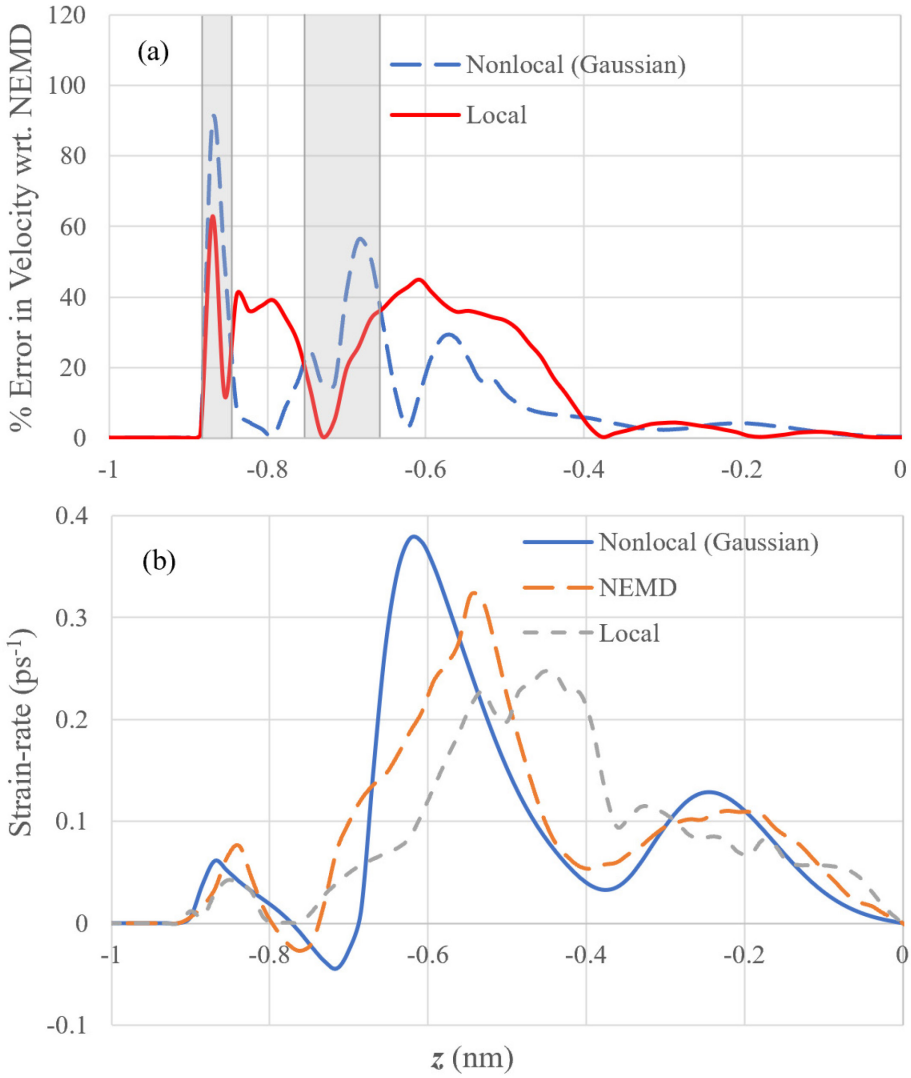

Figure 7: (a) % Error in the Nonlocal (Gaussian) and local velocities w.r.t. the NEMD velocity profile across a half-section of the narrow channel. The red (solid) and blue (dashed) lines are the local and nonlocal error profiles respectively. (b) The strain-rate profile across a half-section of the narrow channel ~~for the velocity profiles in Fig. 6(b)~~. The blue (solid), orange (dashed) and grey (smaller dashed) lines are the nonlocal, reference NEMD and local strain-rate profiles respectively.

V. CONCLUSION

We have considered a transport model to predict gravity-driven flows in nanochannels using nonlocal hydrodynamics. As such velocity profiles contain multiple local extrema, the local shear stress relation is expected to fail and the nonlocality of the system must be stressed on. Although these flows are usually computed using MD simulations, here we use a continuum model with a nonlocal constitutive shear stress relation considering the neighboring strain-rates through their convolution with a position-dependent nonlocal viscosity kernel to do so. We estimate such kernels of the inhomogeneous fluid as isotropic kernels of homogeneous systems by the LADM approach, in conjunction with the STF technique for different kernel expressions, derived by inverting the Gaussian and Lorentzian curve fits of the k-space viscous data to real-space. The proposed nonlocal model captures the key features of the results from NEMD simulations, predicting the characteristic oscillations of the velocities near the fluid-wall interface which form the local extrema in the velocity profile and sign reversals in the strain-rate profile. The nonlocal model shows a much-improved agreement with the observations from MD, when compared to the local Newtonian constitutive theory. Further advances in the development of nonlocal viscosity kernel of non-homogeneous fluids and rectification of the drawbacks of the model presented in this work will provide more efficient continuum methods to model fluid flows in nanoscale confinements.

ACKNOWLEDGEMENTS

A preliminary version of the model presented in this paper was developed by Dr. Bhadauria as part of his PhD thesis at UIUC under the supervision of Dr. Aluru. We gratefully acknowledge support from the National Science Foundation under grant 2140225.

DATA AVAILABILITY STATEMENT

We agree to provide the data that support the findings of this study upon reasonable request.

REFERENCES

[1] D.J. Evans and G.P. Morriss, *Statistical Mechanics of Nonequilibrium Liquids*, Academic Press Limited, New York (1990).

[2] K.P. Travis, B.D. Todd, and D.J. Evans, Physical Review E **55**, 4288 (1997).

[3] J. Zhang, B.D. Todd, and K.P. Travis, Journal of Chemical Physics **121**, 10778 (2004).

[4] E. Akhmatskaya, B.D. Todd, P.J. Daivis, D.J. Evans, K.E. Gubbins, and L.A. Pozhar, Journal of Chemical Physics **106**, 4684 (1997).

[5] I. Bitsanis, S.A. Somers, H.T. Davis, and M. Tirrell, The Journal of Chemical Physics **93**, 3427 (1990).

[6] E. Manias, G. Hadziioannou, and G. ten Brinke, Langmuir **12**, 4587 (1996).

[7] K.P. Travis and K.E. Gubbins, The Journal of Chemical Physics **112**, 1984 (2000).

[8] B.A. Dalton, K.S. Glavatskiy, P.J. Daivis, and B.D. Todd, Journal of Chemical Physics **139**, (2013).

[9] B.A. Dalton, P.J. Daivis, J.S. Hansen, and B.D. Todd, Physical Review E - Statistical, Nonlinear, and Soft Matter Physics **88**, (2013).

[10] K.S. Glavatskiy, B.A. Dalton, P.J. Daivis, and B.D. Todd, Physical Review E - Statistical, Nonlinear, and Soft Matter Physics **91**, (2015).

[11] B.A. Dalton, K.S. Glavatskiy, P.J. Daivis, and B.D. Todd, Physical Review E - Statistical, Nonlinear, and Soft Matter Physics **92**, (2015).

[12] Di. Camargo, J.A. de La Torre, D. Duque-Zumajo, P. Español, R. Delgado-Buscalioni, and F. Chejne, Journal of Chemical Physics **148**, (2018).

[13] D. Camargo, J.A. de La Torre, R. Delgado-Buscalioni, F. Chejne, and P. Español, Journal of Chemical Physics **150**, (2019).

[14] D. Duque-Zumajo, D. Camargo, J.A. de La Torre, F. Chejne, and P. Español, Physical Review E **99**, (2019).

~~[8]~~[15] J. Zhang, B.D. Todd, and K.P. Travis, Journal of Chemical Physics **122**, 2004 (2005).

~~[9]~~[16] P.J. Cadusch, B.D. Todd, J. Zhang, and P.J. Daivis, Journal of Physics A: Mathematical and Theoretical **41**, 1 (2008).

~~[10]~~[17] K.P. Travis, D.J. Searles, and D.J. Evans, Molecular Physics **97**, 415 (1999).

~~[11]~~[18] J.S. Hansen, P.J. Daivis, K.P. Travis, and B.D. Todd, Physical Review E - Statistical, Nonlinear, and Soft Matter Physics **76**, 1 (2007).

~~[12]~~[19] B.D. Todd, J.S. Hansen, and P.J. Daivis, Physical Review Letters **100**, 1 (2008).

~~[13] J.D. Weeks, D. Chandler, and H.C. Andersen, The Journal of Chemical Physics **54**, 5237 (1971).~~

~~[14]~~[20] E.M. Gosling, I.R. McDonald, and K. Singer, Molecular Physics **26**, 1475 (1973).

[21] D. Duque-Zumajo, J.A. de La Torre, J.A. de La Torre, and P. Español, Journal of Chemical Physics **152**, (2020).

[22] I. Bitsanis, J.J. Magda, M. Tirrell, and H.T. Davis, The Journal of Chemical Physics **87**, 1733 (1987).

[23] I. Bitsanis, T.K. Vanderlick, M. Tirrell, and H.T. Davis, The Journal of Chemical Physics **89**, 3152 (1988).

[24] R. Bhadauria, *Multiscale Methods for Transport Phenomena*, Doctoral Dissertation, University of Illinois at Urbana-Champaign (2017).

[25] J.D. Weeks, D. Chandler, and H.C. Andersen, The Journal of Chemical Physics **54**, 5237 (1971).

[26] B.D. Todd and J.S. Hansen, Physical Review E - Statistical, Nonlinear, and Soft Matter Physics **78**, (2008).

~~[15]~~[27] R. Bhadauria and N.R. Aluru, Journal of Chemical Physics **139**, 1 (2013).

~~[16]~~[28] R. Bhadauria, T. Sanghi, and N.R. Aluru, Journal of Chemical Physics **143**, 1 (2015).

~~[17]~~[29] R. Bhadauria and N.R. Aluru, Journal of Chemical Physics **145**, 1 (2016).

~~[18]~~[30] R. Bhadauria and N.R. Aluru, Journal of Chemical Physics **146**, 1 (2017).

~~[19]~~[31] R. Bhadauria and N.R. Aluru, Journal of Chemical Physics **147**, 1 (2017).

~~[20] I. Bitsanis, J.J. Magda, M. Tirrell, and H.T. Davis, The Journal of Chemical Physics **87**, 1733 (1987).~~

~~[21] I. Bitsanis, T.K. Vanderlick, M. Tirrell, and H.T. Davis, The Journal of Chemical Physics **89**, 3152 (1988).~~

~~[22] R. Bhadauria, *Multiscale Methods for Transport Phenomena*, Doctoral Dissertation, University of Illinois at Urbana-Champaign (2017).~~

~~[23]~~[32] W.G. Hoover, Physical Review A **31**, (1985).

[33] S. Bernardi, B.D. Todd, and D.J. Searles, Journal of Chemical Physics **132**, (2010).